ARTICLE IN PRESS

Reference 6

Available online at www.sciencedirect.com

SCIENCE DIRECT

ELSEVIER

Journal of Crystal Growth ▮ (▮▮▮▮) ▮▮▮–▮▮▮

JOURNAL OF CRYSTAL GROWTH

www.elsevier.com/locate/jcrysgro

Transmission electron microscopy study of defect reduction in two-step lateral epitaxial overgrown nonplanar GaN substrate templates

Wei Zhou[a,*], Dawei Ren[b], P.D. Dapkus[a,c]

[a]*Department of Materials Science, University of Southern California, Los Angeles, CA 90089, USA*
[b]*Department of Physics, University of Southern California, Los Angeles, CA 90089, USA*
[c]*Department of Electrical Engineering—Electrophysics, University of Southern California, Los Angeles, CA 90089, USA*

Received 17 September 2004; received in revised form 13 December 2005; accepted 16 December 2005

Communicated by T.F. Kuech

Abstract

Transmission electron microscopy (TEM) is carried out to characterize the extended defect reduction in low-defect nonplanar GaN substrate templates grown by lateral epitaxial overgrowth (LEO). The LEO nonplanar GaN substrate template has a trapezoidal cross section with smooth (0 0 0 1) and $\{1\,1\,\bar{2}\,2\}$ facets. We demonstrate here the dislocation distribution and behavior in both ordinary LEO and two-step LEO. Penetration of threading dislocations (TDs) beyond mask windows is observed in ordinary LEO substrates. In two-step LEO substrates, which utilize the tendency for TDs to bend 90° at certain plane interfaces, only **a** type dislocations with Burgers vector $\mathbf{b}=\frac{1}{3}\langle 1\,1\,\bar{2}\,0\rangle$ are generated in the upper part above the TD bending zone between two mask windows with a density of $\sim 8\times 10^{7}\,\mathrm{cm}^{-2}$, and there are almost no dislocations in the LEO wing region. This approach provides a promising path to produce low-defect GaN substrate templates for high-performance buried heterostructure lasers.

PACS: 68.55.−a; 61.72.Lk; 81.05.Ea; 61.72.Ff; 68.37.−d; 81.15.Gh; 68.37.Lp

Keywords: A1. Dislocation reduction; A1. Threading dislocation; A1. Transmission electron microscopy; A1. TEM; A3. lateral epitaxial overgrowth; A3. LEO; A3. Metalorganic chemical vapor deposition; A3. MOCVD; B2. III–V semiconductors; B1. GaN; B1. Nitrides; B3. Lasers

1. Introduction

GaN and its related alloys have become the most promising wide band gap semiconductor materials for fabricating short wavelength light-emitting diodes and laser diodes (LDs) as well as high-power, high-frequency electronic devices [1]. But typically epitaxially grown III-nitride materials are known to exhibit a high density of dislocations in the 10^{9}–$10^{10}\,\mathrm{cm}^{-2}$ range, owing to the current need to grow on lattice-mismatched substrates [2]. Deterioration of the optical and transport properties of GaN-based films has been attributed to these defects [3,4]. Thus, the reduction of dislocation density in the GaN crystals must be inevitably achieved to obtain a longer lifetime and higher electro-optical properties of LD devices [5]. Recently, lateral epitaxial overgrowth (LEO) has been studied extensively as an approach to efficiently reduce the defect density of the GaN films grown on sapphire where lateral epitaxy occurs over an amorphous dielectric mask [6–8]. Ordinary LEO introduces a high ratio of the lateral to vertical growth rates when regrowth over mask opening begins. Complicated microstructures, such as wing tilting, 90° bending of threading dislocations (TDs), and generation of horizontal dislocations (HDs) have been reported [9,10]. Most recently, two-step planar LEO has successfully reduced dislocation density to the 10^{-6}–$10^{-7}\,\mathrm{cm}^{-2}$ ranges in the lateral epitaxy area [11]. The densities in the GaN template layers are reported in the $10^{8}\,\mathrm{cm}^{-2}$ range for **a** type dislocations with Burgers vector $\mathbf{b}=\frac{1}{3}\langle 1\,1\,\bar{2}\,3\rangle$ and

*Corresponding author. Tel.: +1 213 7404391; fax: +1 213 7406022.
E-mail address: waynezhouw@gmail.com (W. Zhou).

0022-0248/$ - see front matter © 2006 Elsevier B.V. All rights reserved.
doi:10.1016/j.jcrysgro.2005.12.108

Report Documentation Page

Form Approved
OMB No. 0704-0188

1. REPORT DATE	2. REPORT TYPE	3. DATES COVERED
01 JUN 2005	**N/A**	**-**

4. TITLE AND SUBTITLE	5a. CONTRACT NUMBER
Transmission electron microscopy study of defect reduction in two-step lateral epitaxial overgrown nonplanar GaN substrate templates	5b. GRANT NUMBER
	5c. PROGRAM ELEMENT NUMBER
6. AUTHOR(S)	5d. PROJECT NUMBER
	5e. TASK NUMBER
	5f. WORK UNIT NUMBER
7. PERFORMING ORGANIZATION NAME(S) AND ADDRESS(ES) **Department of Materials Science, University of Southern California, Los Angeles, CA 90089, USA**	8. PERFORMING ORGANIZATION REPORT NUMBER
9. SPONSORING/MONITORING AGENCY NAME(S) AND ADDRESS(ES)	10. SPONSOR/MONITOR'S ACRONYM(S)
	11. SPONSOR/MONITOR'S REPORT NUMBER(S)

12. DISTRIBUTION/AVAILABILITY STATEMENT
Approved for public release, distribution unlimited

13. SUPPLEMENTARY NOTES
See also ADM001923.

14. ABSTRACT

15. SUBJECT TERMS

16. SECURITY CLASSIFICATION OF:			17. LIMITATION OF ABSTRACT	18. NUMBER OF PAGES	19a. NAME OF RESPONSIBLE PERSON
a. REPORT	b. ABSTRACT	c. THIS PAGE			
unclassified	**unclassified**	**unclassified**	**UU**	**7**	

a+**c** type dislocations with Burgers vector $\mathbf{b}=\frac{1}{3}\langle 1\,1\,\bar{2}\,3\rangle$, whereas the density of **c** type dislocations with Burgers vector $\mathbf{b}=\langle 0\,0\,0\,1\rangle$ can approach the $10^7\,\mathrm{cm}^{-2}$ range at most [12].

In a previous study in the InGaAs system, an approach was developed to produce nonplanar substrate templates on which low threshold lasers offering good optical confinement and current confinement were formed [13]. A similar idea is now being pursued in the InGaN system along with the LEO technique. Our study results have already shown that with the two-step LEO technique, enhanced Indium incorporation as well as the reduction of Indium phase segregation can be achieved in the single InGaN quantum well grown on nonplanar LEO GaN, which is much superior to the counterpart on planar GaN [14].

In this article, we used cross-sectional transmission electron microscopy (TEM) to investigate the defect structures in the nonplanar GaN mesas grown by our two-step method in comparison with the ordinary LEO. A comparison of growth procedures is reviewed in Section 2. In Section 3, we present TEM results on both LEO methods for nonplanar substrates. This section also includes a discussion of dislocation propagation and category distributions in both the TD bending layer and the post-bending layer of two-step nonplanar substrates, with the **g*b** dark field analysis.

2. Experimental procedure

The growth of LEO GaN was carried out by metalorganic chemical vapor deposition (MOCVD) in a Thomas Swan close-spaced showerhead vertical reactor. Hydrogen was used as the carrier gas. Trimethylgallium (TMGa) and pure NH_3 were used as the III and V column sources. Growth pressure was kept at 200 Torr. GaN planar buffers (2 μm thick) were grown on (0 0 0 1) sapphire substrates using a conventional two-step process [15]. Samples were then coated with 100 nm thick SiN_x by plasma enhanced CVD (PECVD). Stripe patterns were created on these GaN buffers using conventional photolithography and CF_4 reactive ion etching. The pattern openings were chosen to be along the sapphire $[1\,1\,\bar{2}\,0]$ direction in order to get $[1\,\bar{1}\,0\,0]$ LEO GaN stripes [16].

Ordinary LEO GaN growth started with stripe patterned GaN. Although the total growth was performed continuously, its morphological change could be divided into three morphological stages, as indicated in Fig. 1(a). In stage I, two separate sub mesas of LEO GaN were selectively grown in the opening window region. Two adjacent facets started to merge in stage II. Lateral overgrowth in stage III helped to form smooth mesa top plane. There was no growth parameter change throughout the entirely LEO growth (growth temperature of 1080 °C and V/III ratio of 2500).

Modified LEO GaN growth differed from the ordinary growth described above in that, in morphological stage II, not only did two adjacent facets start to coalesce but also the top c planes of two sub-mesas disappeared completely by establishing the proper growth conditions, as shown in Fig. 1(b). The mask design was kept the same as the ordinary LEO. In this case, however, the growth conditions were changed during growth: First, growth parameters enhancing [0 0 0 1] growth rate (growth temperature of 1060 °C and V/III ratio of 630) were adopted to form triangular cross-sectional mesas with the disappearance of the (0 0 0 1) facet, corresponding to stage I & II; Second, in stage III, the growth parameters were changed to enhance lateral growth rate (growth temperature of 1080 °C and V/III ratio of 2500), facilitating complete coalescence of two adjacent triangular LEO sub-mesas. The purpose of this sequence of procedures was to bend the TDs to reduce the dislocation density in the device active region that is to be formed on the mesa top, based on our observation of the TD bending phenomenon, as seen in Fig. 2. The detailed growth methods will be presented in another paper.

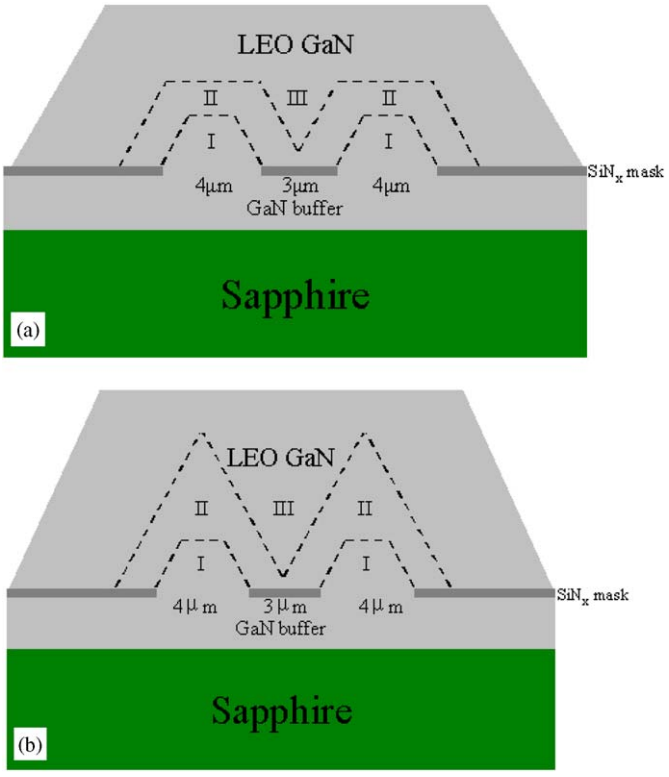

Fig. 1. Schematics of nonplanar LEO GaN substrate growth process with the same mask design along the $[1\,\bar{1}\,0\,0]$ azimuth. (a) Ordinary LEO GaN growth divided into three stages. (b) Modified LEO GaN growth divided into three stages, where the vertical favored growth condition changed to the lateral enhanced growth condition after stage II. Dashed lines represent the shapes of respective stages.

Cross-sectional TEM samples were prepared by mechanical tripod polishing [17] and Ar^+-ion milling at 5 kV. The TEM investigation was carried out on either a Philips EM420 operating at 120 kV or an Akashi 002B operating at 200 kV.

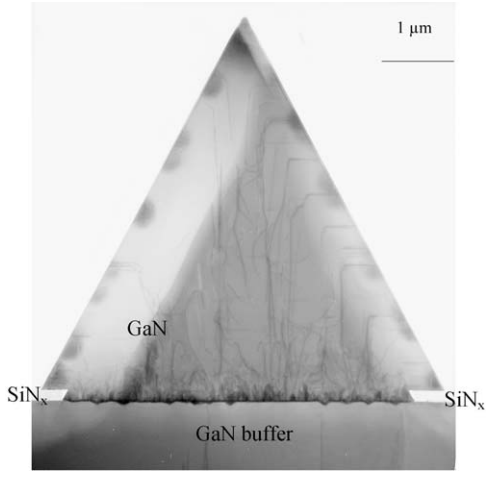

Fig. 2. Bright-field cross-sectional TEM image of LEO GaN over a SiN_x mask window along the $[1\,1\,\bar{2}\,0]$ zone axis. TDs were observed to bend 90° near the inclined sidewall to adopt a horizontal direction in the basal plane.

3. Results and discussion

3.1. Conventional single-step nonplanar LEO

Lateral overgrowth is favored in conventional LEO, and the TDs that emerge from the mask windows travel directly to the mesa top plane. This is shown in Fig. 3, which includes cross-sectional TEM images along the $[1\,\bar{1}\,0\,0]$ zone axis of a mesa formed by conventional LEO. The TD density is greatly reduced in the lateral overgrown region because the amorphous SiN_x mask prevents growth on the GaN below and the GaN that is formed results only from lateral growth. In the region above the windows, TDs propagate from the buffer substrate along *c*-axis up to the mesa surface with almost the same TD density as in the buffer. There are almost no defects in the LEO region and coalescence region except a few dislocations to accommodate strains associated with the central void.

3.2. Modified nonplanar LEO

The observation of dislocation bending in triangular shaped mesas of the nonplanar LEO GaN illustrated in Fig. 2 motivated us to apply a two-step LEO to form the nonplanar LEO template. In the first step, the growth rate of the inclined $\{1\,1\,\bar{2}\,2\}$ facets is slow and they dominate the resultant morphology of the mesa. This growth condition is maintained until the $(0\,0\,0\,1)$ facet disappears with only $\{1\,1\,\bar{2}\,2\}$ facets left, as shown in Fig. 4. Then, the growth condition is changed to increase the growth rate of $\{1\,1\,\bar{2}\,2\}$ facets relative to that of the $(0\,0\,0\,1)$ facet, until a smooth coalesced nonplanar GaN mesa is obtained. The distribution and behavior of the dislocations in this substrate will be presented below.

3.2.1. The first step nonplanar LEO

A typical strip cross section at the end of the first growth step is shown along the $[1\,\bar{1}\,0\,0]$ zone axis in Fig. 4. As expected, TDs under the masks are blocked by the masks while TDs through the mask windows are observed to bend 90° towards the inclined $\{1\,1\,\bar{2}\,2\}$ facets at least 1.5 μm beneath the peaks. After bending, these TDs propagate horizontally in the $(0\,0\,0\,1)$ basal plane. As a result, almost none of the TDs reach the top plane after complete coalescence of both sub-LEO stripes. Some TDs adopt abrupt bending while other TDs may propagate along a gradually changing route before entering the basal plane.

Dashed lines in Fig. 4 connect the bending points of the TDs, showing that bending phenomenon happens first to the TDs at the window edge and last to those at the window center. None of the TDs located in the center of the pyramid were observed to thread up to the top without bending in any of our TEM samples. The dashed lines actually portrait the trajectories of the edges between the C top facet and inclined $\{1\,1\,\bar{2}\,2\}$ facets as they move along in this growth step, with an angle of ~75° (governed by growth conditions) to the basal plane. This phenomenon was explained by image force theory [18]. As long as a vertical dislocation line gets close enough to the edge trajectories, it will be attracted by the image force and bent toward the new $\{1\,1\,\bar{2}\,2\}$ facets to adopt a new horizontal direction in the basal plane, because of different interactions between the surfaces and the dislocation line. Thus, TD's bending is associated with the stress field relaxation. The moving facet edges could also be contributing to the TD's bending. Detailed dislocation characterization will be presented in the next section.

3.2.2. The second step nonplanar LEO

A typical cross-sectional TEM image of the whole nonplanar mesa at the end of the second step is shown in Fig. 5, which is a collage of five micrographs. TDs that penetrate through the mask opening are only able to thread upwards for 8.2 μm before they bend 90° and annihilate at the growing free $\{1\,1\,\bar{2}\,2\}$ surface. Those TDs bend towards the center seam between islands and most of them annihilate here. Thus, the TD bending layer is referred to as the epitaxial layer containing all the bending TDs above masks, which is around 8.2 μm above the masks; while the post-bending layer is considered to be the materials that extends from the top of TD bending layer to the free mesa top surface. The surface dislocation density is abruptly decreased to $\sim 8 \times 10^7 \mathrm{cm}^{-2}$ between the two mask openings and is almost zero in the LEO wing region. Many horizontal dislocation (HD) segments exist in the wing area of the TD bending layer. There are also many small remnant dislocations (RDs) mainly pointing upward in the post-bending layer in and between two windows.

The **g*b** dark field analysis has been applied to characterizing various dislocations distributed in the trapezoidal mesa. The $\mathbf{g} = (1\,1\,\bar{2}\,0)$, $(0\,0\,0\,2)$ and $(1\,1\,\bar{2}\,\bar{2})$ dark field TEM images are shown in Fig. 6, corresponding

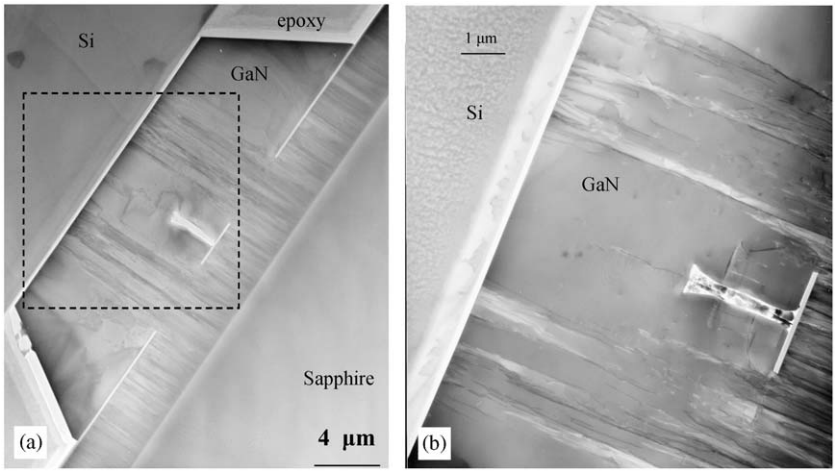

Fig. 3. Bright-field cross-sectional TEM image of Ordinary LEO nonplanar GaN along the [1 $\bar{1}$ 0 0] zone axis: (a) dislocation distribution in a typical GaN mesa; (b) a higher magnification view of the boxed area of (a). Si wafer is used as a thickness indicator in the TEM sample preparation.

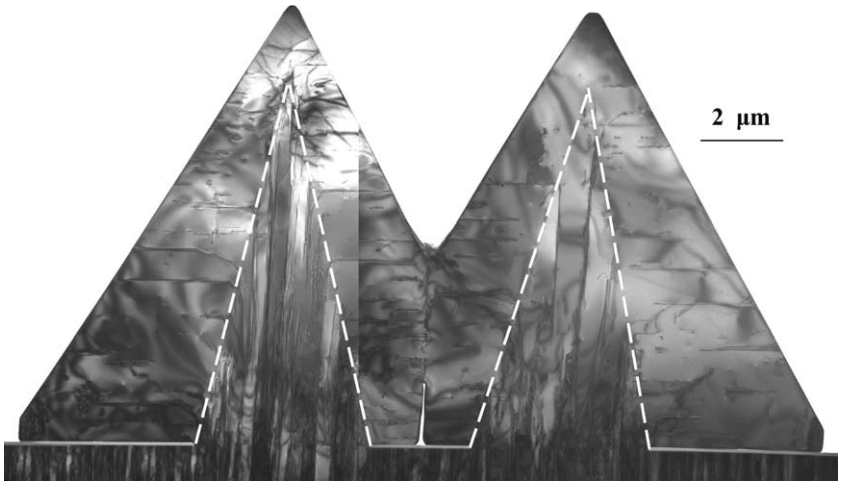

Fig. 4. Bright-field cross-sectional collaged TEM image of modified LEO nonplanar GaN at the end of the 1st step along the [1 $\bar{1}$ 0 0] zone axis: Two adjacent GaN pyramids begin to merge; all TDs have been bent in 90°; dashed lines connect the bending points of the TDs.

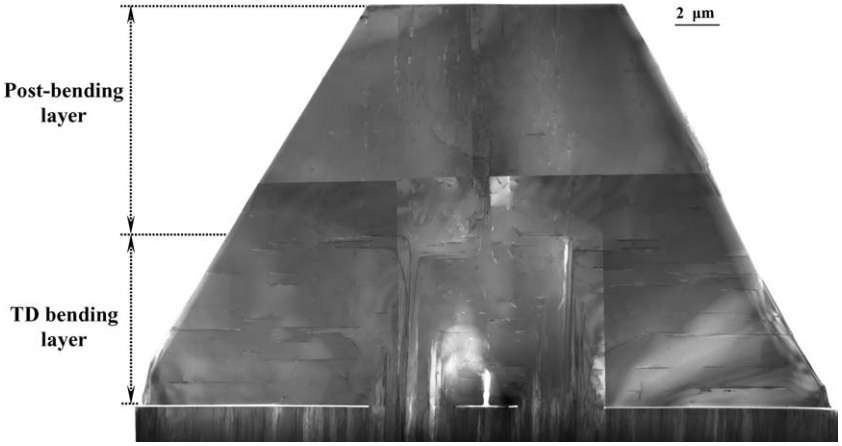

Fig. 5. Bright-field cross-sectional collaged TEM image of modified LEO nonplanar GaN at the end of the second step along the [1 $\bar{1}$ 0 0] zone axis.

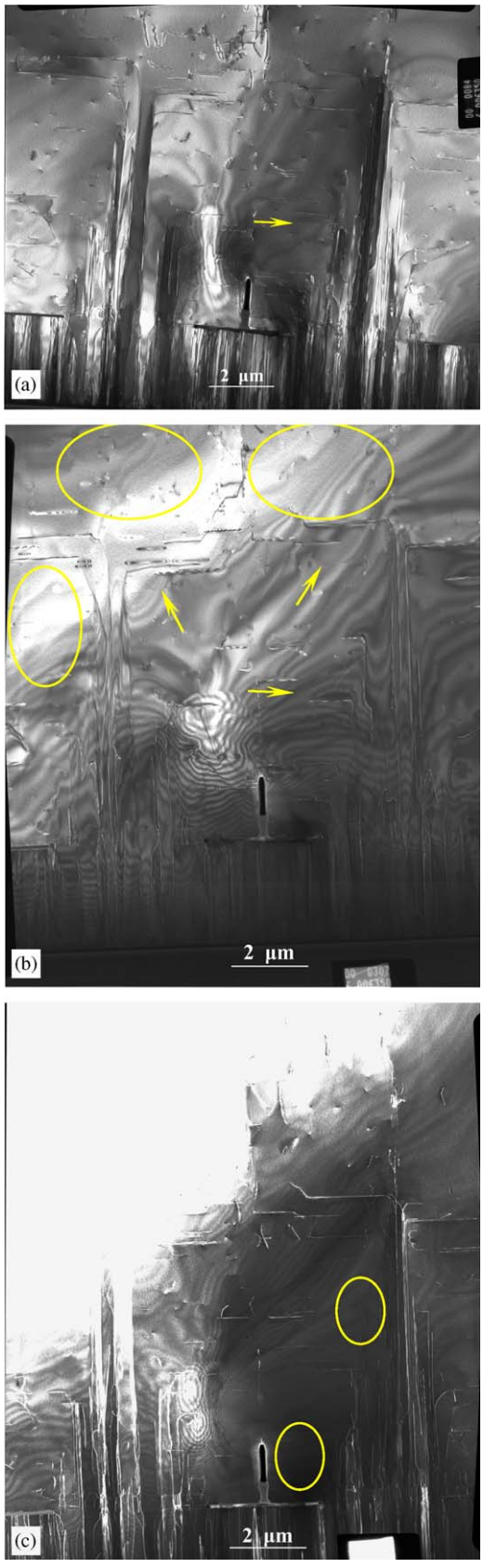

Fig. 6. Dark-field cross-sectional TEM image for the TD bending layer center part of the modified LEO nonplanar GaN at the end of the second step near the $[1\,\bar{1}\,0\,0]$ zone axis. (a) $\mathbf{g}=(1\,1\,\bar{2}\,0)$; (b) $\mathbf{g}=(0\,0\,0\,2)$; (c) $\mathbf{g}=(1\,1\,\bar{2}\,\bar{2})$. Arrows and circles point out where the extinguished dislocations are located.

to the center part of the TD bending layer. Most of the bending TDs are in contrast in both of the $\mathbf{g}=(1\,1\,\bar{2}\,0)$ & $(0\,0\,0\,2)$ dark fields and hence should be mixed $\mathbf{a}+\mathbf{c}$ type dislocations with Burgers vector $\mathbf{b}=\frac{1}{3}\langle 1\,1\,\bar{2}\,3\rangle$, which is confirmed by the observation that many dislocations (in the circles area) lose contrast in the $\mathbf{g}=(1\,1\,\bar{2}\,\bar{2})$ dark field (Fig. 6(c)). The bending dislocation (indicated by an arrow in Fig. 6(a)) that is extinguished in the $(1\,1\,\bar{2}\,0)$ dark field should be a **c**-type dislocation with Burgers vector $\mathbf{b}=\langle 0\,0\,0\,1\rangle$. Some bending dislocations and short dislocations above the bending layer should be **a** type dislocations with Burgers vector $\mathbf{b}=\frac{1}{3}\langle 1\,1\,\bar{2}\,0\rangle$ inside the circles or pointed by arrows in Fig. 6(b), since they lose contrast or have only residual contrast in the $(0\,0\,0\,2)$ dark field. In the bending layer, the density of **a**-type dislocations are higher than that of **c**-type dislocations.

There are stripe-like domains with different contrasts at the mask openings in Figs. 6(a) and (c), delineated by low-angle grain boundary (LAGB) intersections. The different diffraction contrast found in the $\mathbf{g}=(1\,1\,\bar{2}\,0)$ dark field itself excludes the possibility of inversion twins. We attribute this sub-domain phenomenon to the coalescence of slightly misoriented domains during growth. Regions of the substrate that are exactly at the Bragg condition will have a brighter contrast than those slightly off-Bragg. The domains on either side of the LAGB have different orientations.

The $\mathbf{g}=(1\,1\,\bar{2}\,0)$ and $(0\,0\,0\,2)$ dark field TEM images are shown in Fig. 7, corresponding to the post-bending layer, which happens to be where our future device will be situated. There are short RDs nearly vertical to the c top surface in the $(1\,1\,\bar{2}\,0)$ dark field. Almost all of them lose contrast in the $(0\,0\,0\,2)$ dark field (Fig. 7(b)) and hence should be **a** type dislocations. These dislocations are not as straight as the TDs in the bending layer and distributed mainly between the two mask openings. These **a** type dislocations propagate in the $\{1\,\bar{1}\,0\,0\}$ planes for a certain short length and then gradually slant outside the sample foil at either end, since dashed lines appear in one or both ends of these dislocation lines while constant contrast is maintained in the center part of these dislocation lines. No loop is found here when the sample is tilted around the $[1\,1\,\bar{2}\,0]$ or $[0\,0\,0\,1]$ axis by 30°. The disorientation between two coalescing fronts and extended internal stress from below are believed to give rise to the formation of these **a** type dislocations. A few mixed $\mathbf{a}+\mathbf{c}$ type dislocations exhibiting in both dark field images are located close to the bending layer.

The $\mathbf{g}=(0\,1\,\bar{1}\,\bar{2})$ and $(0\,0\,0\,\bar{2})$ dark field TEM images shown in Fig. 8 are corresponding to the LEO region of the nonplanar GaN LEO substrate sample near the $[2\,\bar{1}\,\bar{1}\,0]$ zone axis. It is observed that the small dot defects of the LEO region in the $[1\,\bar{1}\,0\,0]$ zone axis are actually edge-on dislocations lying on the basal plane with the same direction as the zone axis. Those tiny edge-on dislocations (inside the circle) in the LEO region above bending dislocations lose contrast in the $(0\,0\,0\,\bar{2})$ dark field and thus should be **a** type dislocations.

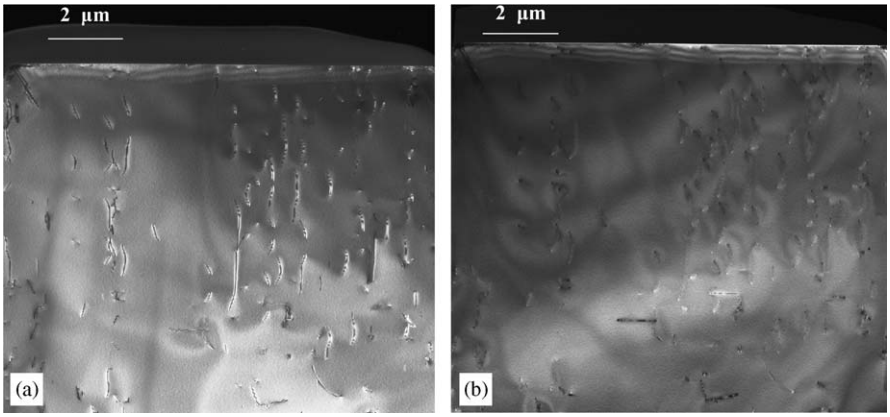

Fig. 7. Dark-field cross-sectional TEM image for the post-bending layer of the modified LEO nonplanar GaN at the end of the second step near the $[1\,\bar{1}\,0\,0]$ zone axis. (a) $\mathbf{g} = (1\,1\,\bar{2}\,0)$; (b) $\mathbf{g} = (0\,0\,0\,2)$.

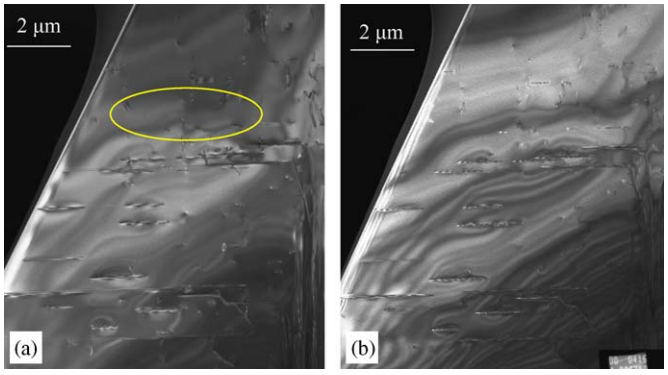

Fig. 8. Dark-field cross-sectional TEM image for the LEO region of the modified LEO nonplanar GaN at the end of the second step near the $[2\,\bar{1}\,\bar{1}\,0]$ zone axis. (a) $\mathbf{g} = (0\,1\,\bar{1}\,\bar{2})$; (b) $\mathbf{g} = (0\,0\,0\,\bar{2})$. The circle point out where the edge-on dislocations reside.

In conclusion, the distribution of dislocations in nonplanar GaN LEO substrate mesas are identified as the following within two sub-layers defined above:

(i) TD bending layer (the epitaxial layer containing all the bending TDs above masks): a high density of TDs penetrating through the mask windows, which have been bent by 90°, are composed of mostly mixed **a**+**c** type $\mathbf{b} = \frac{1}{3}\langle 1\,1\,\bar{2}\,3\rangle$ dislocations, with a smaller number of **a** type $\mathbf{b} = \frac{1}{3}\langle 1\,1\,\bar{2}\,0\rangle$ dislocations and rare **c** type $\mathbf{b} = \frac{1}{3}\langle 0\,0\,0\,1\rangle$ dislocations. In the wing area, there are only HD segments, which consist of mostly bent-over TDs intersected by the foil plane.

(ii) Post-bending layer (from the top of TD bending layer to the free mesa top surface): **a** type $\mathbf{b} = \frac{1}{3}\langle 1\,1\,\bar{2}\,0\rangle$ dislocations with a low density of $\sim 8 \times 10^7\,\mathrm{cm}^{-2}$ are distributed mainly between the two mask windows with either end gradually propagating out of the sample foil. And there is almost no dislocation in the LEO wing region. The finding of small **a** type dislocations in the basal plane also confirms the versatile propagation directions of these **a** type dislocations. Dislocations that can threaten laser device performance are mainly **a** type dislocations. Further investigation of this unique dislocation distribution will be presented separately.

4. Summary

In summary, we have successfully applied two-step LEO to fabricating coalesced low-defect nonplanar GaN substrate templates for high performance device fabrication. In contrast, with the continuous TDs in the conventional LEO substrates, a TD 90° bending layer has significantly prevented TDs from disturbing the upper layer used for device fabrication. Cross-sectional TEM has confirmed the existence of three types of dislocations in the TD bending layer, consisting of many mixed **a**+**c** type dislocations, some **a** type dislocations and few **c** type dislocations. The resultant nonplanar GaN post-bending layer has only **a** type dislocations generated between two mask windows with a density of $\sim 8 \times 10^7\,\mathrm{cm}^{-2}$, which is three orders of magnitude lower than that of bulk GaN ($\sim 10^{10}\,\mathrm{cm}^{-2}$). The formation of **a** type dislocations is attributed to the disorientation between two coalescing fronts and internal stress. Further work is underway to gain more knowledge and control of **a** type dislocations in the over-layer and to assess their impact on our device properties.

Acknowledgments

This work is supported by DARPA. The authors are grateful to Dr. Goo for fruitful discussion.

References

[1] Y.-F. Wu, B.P. Keller, P. Fini, S. Keller, T.J. Jenkins, L.T. Kehias, S.P. DenBaars, U.K. Mishra, IEEE Electron Dev. Lett. 19 (1998) 50.
[2] F.A. Ponce, MRS Bull. Feb. 51 (1997) 45.
[3] S. Keller, B.P. Keller, Y.F. Wu, B. Heying, D. Kapolnek, J.S. Speck, U.K. Mishra, S.P. DenBaars, Appl. Phys. Lett. 68 (1996) 1525.
[4] N.G. Weimann, L.F. Eastman, D. Dharanipal, H.M. Ng, T.D. Moustakas, J. Appl. Phys. 83 (1998) 3656.

[5] S. Nakamura, M. Senoh, S. Nagahama, N. Iwasa, T. Yamada, T. Matsushita, H. Kiyoku, Y. Sugimoto, T. Kozaki, H. Umemoto, M. Sano, K. Chocho, Jpn. J. Appl. Phys. Lett. 37 (1998) 309.
[6] H. Marchand, X.H. Wu, J.P. Ilbbetson, P.T. Fini, P. Kozodoy, S. Keller, J.S. Speck, S.P. DenBaars, U.K. Mishra, Appl. Phys. Lett. 73 (1998) 747.
[7] B. Beaumont, M. Vaille, G. Nataf, A. Bouillé, J.-C. Guillaume, P. Vennéguès, S. Haffouz, P. Gibart, MRS Internet J. Nitride Semicond. Res. 3(Art 20) (1998).
[8] K. Horibuchi, N. Kuwano, H. Miyake, K. Hiramatsu, J. Crystal Growth 1070 (2002) 237.
[9] A. Sakai, H. Sunakawa, A. Kimura, A. Usui, Appl. Phys. Lett. 76 (2000) 442.
[10] K. Horibuchi, N. Kuwano, K. Oki, Y. Kawaguchi, N. Sawaki, K. Hiramatsu, Phys. Stat. Sol. A 180 (2000) 171.
[11] P. Vennéguès, B. Beaumont, V. Bousquet, M. Vaille, P. Gibart, J. Appl. Phys. 87 (2000) 4175.
[12] P. Vennéguès, B. Beaumont, S. Haffouz, M. Vaille, P. Gibart, J. Crystal Growth 187 (1998) 167.
[13] Hanmin Zhao, Yong Cheng, Michael H. MacDougal, Gye-Mo Yang, P.D. Dapkus, IEEE Photonics Technol. Lett.7 (1995) 6.
[14] Wei Zhou, Dawei Ren, P.D. Dapkus, J. Crystal Growth 283 (1–2) (2005) 31.
[15] B.P. Keller, S. Keller, D. Kapolnek, W.N. Jiang, Y.-F. Wu, H. Masui, X.H. Wu, B. Heying, J.S. Speck, U.K. Mishra, S.P. DenBaars, J. Electron. Mater. 24 (1992) 1707.
[16] X.H. Wu, L.M. Brown, D. Kapolnek, S. Keller, B. Keller, S.P. DenBaars, J.S. Speck, J. Appl. Phys. 80 (1996) 3228.
[17] S.J. Klepeis, J.P. Benedict, R.M. Anderson, A Grinding/Polishing Tool for TEM Sample Preparation, Mater. Res. Soc. Proc. 115, Pittsburgh, PA USA, 179 (1987)
[18] Z. Liliental-Weber, M. Benamara, W. Swider, J. Washburn, J. Park, P.A. Grudowski, C.J. Eiting, R.D. Dupuis, MRS Internet J. Nitride Semicond. Res. 4s1 (1999) 4.6.